RSC Advances

PAPER

View Article Online
View Journal | View Issue

Check for updates

Cite this: *RSC Adv.*, 2025, **15**, 27033

Synergistic, theoretical, and experimental study of the interaction of a tri-heterometallic polymer with bovine liver catalase†

Narges Lashkarzade,[a] Fereshteh Shiri, *[a] Somaye Shahraki, *[a] Zohreh Razmara [a] and Mostafa Heidari Majd[b]

Reactive oxygen species (ROS) modulate redox balance and cellular processes such as proliferation, angiogenesis, metabolism, immune modulation, and metastasis. Metal-based polymeric complexes have shown potential in disrupting oxidative pathways relevant to tumor development. A comprehensive investigation was conducted on the interaction between a Cu/Mn/Na polymer and catalase, as well as its cytotoxic behavior. The compound exhibited notable antioxidant properties, achieving 61.2% inhibition of the DPPH radical at 125 μM after 60 min. Additionally, the polymer enhanced bovine liver catalase (BLC) activity by up to 138.9% at 7.7×10^{-6} M, with a moderate binding constant in the range of 10^4 M^{-1}. Fluorescence analyses revealed a static quenching mechanism, and molecular docking revealed hydrogen bonding and van der Waals forces to be the key stabilizing interactions. Conformational analyses demonstrated significant structural alterations in BLC upon polymer interaction. The MTT assay revealed considerable antiproliferative effects against colon carcinoma (HCT116) cells, with activity comparable with that of cisplatin at higher concentrations. Importantly, unlike cisplatin, the polymer exhibited minimal toxicity towards normal cells (NIH/3T3), suggesting its potential as an anticancer agent. These findings indicate the potential of the polymer as a redox-modulating therapeutic agent with promising anticancer properties.

Received 23rd April 2025
Accepted 15th July 2025

DOI: 10.1039/d5ra02826d

rsc.li/rsc-advances

Open Access Article. Published on 29 July 2025. Downloaded on 12/6/2025 10:08:35 PM.
This article is licensed under a Creative Commons Attribution-NonCommercial 3.0 Unported Licence.

Introduction

Organometallic polymers or metallopolymers, which were discovered in the 20th century, have attracted the attention of many researchers due to the unique combination of organic and inorganic components in a macromolecular system. In these compounds, an advantage can be achieved by simultaneously combining the important properties of metals (*e.g.*, electronic, catalytic, magnetic and radioactive properties) and important properties of organic parts (*e.g.*, mechanical and processing properties of polymer frameworks).[1,2] About 30 metals have been used in polymer systems. According to the nature and structure of the polymer and metal used (which are usually bridged by covalent or supramolecular bonds), the metal used is usually a transition metal.[3] Various biological functions have been reported for metal-containing polymers, and they can be classified into four groups:[1] metal polymers as drug-delivery systems;[2] metal polymers as drugs and biocides;[3] metal polymers for bioassays;[4] metal polymers for bioimaging. Most drug-delivery systems use redox chemistry or the dynamic covalent bonding chemistry of metals. The main focus of this research is the function of metal polymers as antioxidants, anticancer, antiviral and antimicrobial agents, and biocides, and their use in photodynamic therapy and radiotherapy.[3]

The role of catalase in cancer is undeniable, making it one of the most significant biological molecules. Its interaction with drugs and metallodrugs is particularly intriguing and has become a focal point of research. Catalase is an enzyme primarily found in the liver of animals and plays a crucial part in the antioxidant defense system. Its main function is to break down hydrogen peroxide (H_2O_2) into water and oxygen, thereby preventing cellular damage caused by reactive oxygen species (ROS).[4] Excessive accumulation of ROS during cellular metabolism can lead to oxidative stress, a condition linked to the development of cancer, neurodegenerative disorders, and cardiovascular diseases. Given its essential role in regulating oxidative stress, catalase has emerged as a promising target in cancer therapy. Researchers are actively exploring various catalase-based approaches to inhibit or enhance its activity as a potential therapeutic strategy.[5] Organometallic polymers possess a wide variety of coordination patterns and structural configurations, along with multiple oxidation states and distinctive thermodynamic and kinetic properties. These characteristics play a crucial part in enhancing their efficacy and safety if utilized as chemotherapeutic agents.

[a]*Department of Chemistry, University of Zabol, Zabol, Iran. E-mail: fereshteh.shiri@gmail.com; Fereshteh.shiri@uoz.ac.ir; Fax: +98 5431232186; Tel: +98 5431232186*
[b]*Department of Medicinal Chemistry, Faculty of Pharmacy, Zabol University of Medical Sciences, Zabol, Iran*

† Electronic supplementary information (ESI) available. See DOI: https://doi.org/10.1039/d5ra02826d

© 2025 The Author(s). Published by the Royal Society of Chemistry

Open Access Article. Published on 29 July 2025. Downloaded on 12/6/2025 10:08:35 PM.
This article is licensed under a Creative Commons Attribution-NonCommercial 3.0 Unported Licence.

The present study involved the synthesis and detailed analyses of a polymer incorporating copper, manganese, and sodium elements, as outlined by Razmara *et al.*[6] The free radical-scavenging ability of the compound was examined *via* a ˙DPPH assay to determine its antioxidant efficacy. Additionally, its interaction with bovine liver catalase (BLC) was scrutinised through a combination of spectroscopic methods, molecular dynamics and molecular-docking simulations. We systematically explored thermodynamic and binding characteristics, in addition to assessing alterations in enzymatic activity and protein conformation. These outcomes may help to advance the rational design of next-generation polymer-based metallodrugs with improved therapeutic potential.

Results and discussion

Crystal structure of the polymer

An ORTEP diagram showing the molecular structure of the title Cu/Mn/Na polymer is presented in Fig. 1. The intermolecular (Fig. 2a) and intramolecular (Fig. 2b) hydrogen bonds of the Cu/Mn/Na polymer are also disclosed. As shown in Fig. 2a, the crystal packaging of the polymer exhibited extensive O···H···O intramolecular hydrogen bonds between coordinated water molecules (which act as donors) and the oxygen atoms of the carboxylate groups (which act as acceptors). Extensive intermolecular hydrogen bonds were also formed in this polymer (Fig. 2b). Extensive intra- and intermolecular hydrogen bonds in our the molecular structure of our polymer led to structural stabilization and formation of a three-dimensional (3D) polynuclear network.

Monitoring changes in catalase activity

Given the antioxidant characteristics of the Cu/Mn/Na polymer, its influence on the catalytic activity and structural integrity of BLC was investigated. Enzymatic activity was monitored by measuring H_2O_2 decomposition *via* UV-visible spectrophotometry at 240 nm (the characteristic absorption wavelength of H_2O_2). In the experimental setup, a constant concentration of BLC (1.0×10^{-8} M) and H_2O_2 (55.5×10^{-3} M) was incubated with varying concentrations of the polymer for 3 min.

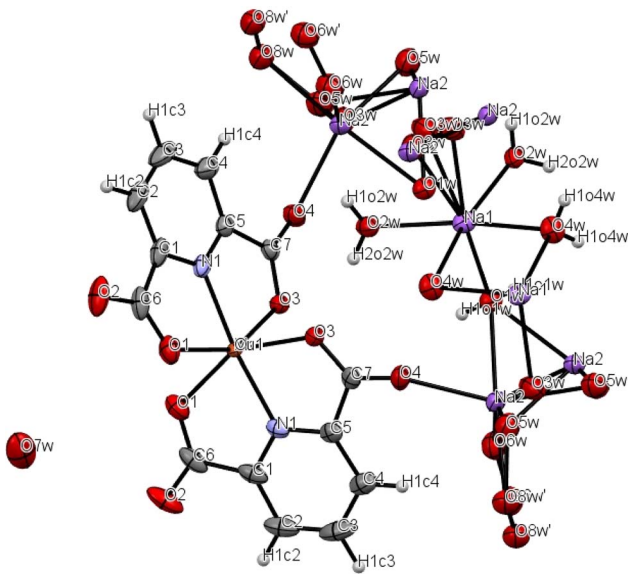

Fig. 1 ORTEP diagram showing the molecular structure of the title Cu/Mn/Na polymer.

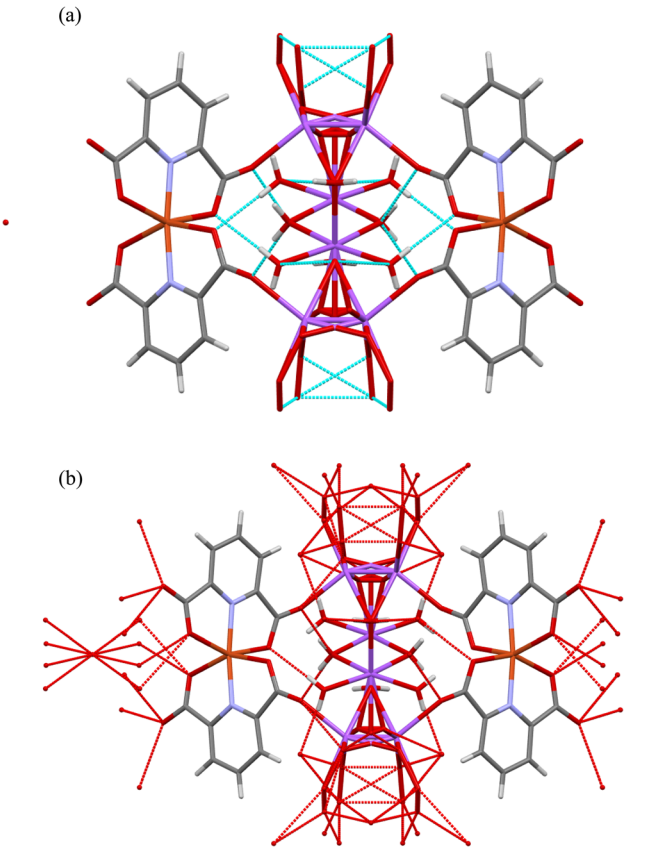

Fig. 2 (a) Intramolecular and (b) intermolecular hydrogen bonds in the crystal structure of the Cu/Mn/Na polymer.

The effect of different polymer concentrations (ranging from 0 to 7.7×10^{-6} M) on catalase activity is illustrated in Fig. 3. Increasing the polymer concentration in the BLC-H_2O_2 system enhanced the efficiency of the enzyme in catalyzing H_2O_2 decomposition. Experiments[7] have shown that H_2O_2 concentrations exceeding 55.5×10^{-3} M can inactivate catalase through a "suicide inhibition" mechanism, so this threshold was selected as the maximum substrate concentration for our study. BLC activity reached 138.9% after interacting with the Cu/Mn/Na polymer (at a concentration of 7.7×10^{-6} M). The interaction of various compounds with catalase has been reported. Some of these compounds have enhanced the activity of the enzyme, and some have acted as inhibitors for catalase and reduced the catalytic activity.[8–13] Enzyme activity can be increased by several factors related to enzyme kinetics. These include increasing temperature (up to a point), substrate concentration (until saturation), and enzyme concentration (up to substrate saturation). Other factors such as pH, cofactors, as well as the presence of activators or inhibitors also have crucial roles.

© 2025 The Author(s). Published by the Royal Society of Chemistry

Open Access Article. Published on 29 July 2025. Downloaded on 12/6/2025 10:08:35 PM.
This article is licensed under a Creative Commons Attribution-NonCommercial 3.0 Unported Licence.

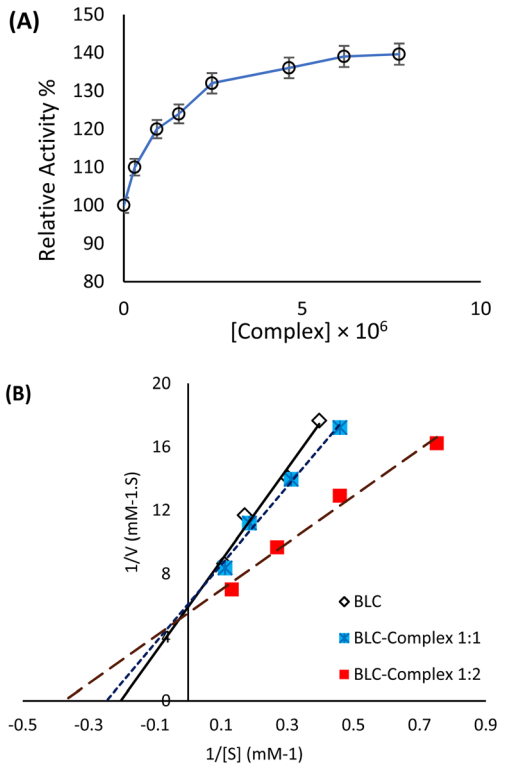

Fig. 3 (A) Catalase activity changes in the presence of the Cu/Mn/Na polymer. [BLC] = 1.0 × 10^{-8} M, [polymer] = (0–7.7 × 10^{-6} M). (B) Lineweaver–Burk plots for the BLC-Cu/Mn/Na polymer. [BLC] = 1.0 × 10^{-8} M and [Cu/Mn/Na polymer] = (1.0 and 2.0 × 10^{-8} M).

Kinetic parameters of the BLC reaction

In order to more accurately evaluate the function of the Cu/Mn/Na polymer on the catalytic activity of catalase, some kinetic parameters such as the Michaelis–Menten constant (K_m) and the reaction maximum rate (V_{max}) were obtained with the help of Lineweaver–Burk plots (Fig. 3B and Table S1†). K_m values for the Cu/Mn/Na polymer at various concentrations decreased compared with that of the control (free BLC) solution. This finding suggested that the Cu/Mn/Na polymer could activate the catalytic function of catalase.[14] Enzyme activators increase the rate of enzyme-catalyzed reactions. They can be divided into two types: cofactors and allosteric activators. Cofactors are often metal ions or organic molecules that bind to the enzyme and enhance its activity. Allosteric activators bind to a site on the enzyme distinct from the active site, inducing a conformational change that increases the affinity of the enzyme for its substrate or its catalytic efficiency. This classification was also made by Saboury.[15] Activation of an enzyme can be achieved by increasing the substrate binding affinity to the enzyme ($\alpha < 1$) and/or increasing the catalytic constant (k_p) to the value $k_p' = \beta k_p$. Saboury classified the different types of reversible activation by the role of two parameters: α and β.[15] Based on the type of graph obtained in Fig. 3B, it seems that the role of increasing the reaction rate and the β factor was more effective. Therefore, it can be predicted that the Cu/Mn/Na polymer as a cofactor led to an improvement in catalase activity.

Fluorescence characteristics of catalase upon polymer binding

The intrinsic fluorescence properties of proteins mainly originate from aromatic amino acids such as tryptophan (Trp), tyrosine (Tyr), and phenylalanine (Phe). Trp and Tyr are the dominant contributors in catalase. These residues are sensitive to alterations in their microenvironment, making them valuable indicators of conformational changes. In the present study, the native fluorescence of BLC was evaluated under varying concentrations of the Cu/Mn/Na polymer at 303, 310, and 317 K. The unmodified BLC exhibited a broad emission maximum at 345 nm upon excitation at 280 nm. As shown in Fig. 4, incremental addition of the polymer resulted in progressive quenching of fluorescence intensity, indicative of formation of a non-fluorescent complex. However, the absence of a shift in the emission maximum suggested that the polarity around Trp and Tyr residues remained relatively unchanged, implying that the quenching arose primarily from complexation rather than environmental perturbation.[16]

Fluorescence quenching in proteins generally follows two primary mechanisms: dynamic and static. The former arises from collisions between the fluorophore and quencher while the fluorophore is in its excited state. Static quenching involves the formation of a stable, non-emissive complex in the ground state. In some cases, both mechanisms may contribute simultaneously. These can be differentiated based on their thermal responses. Dynamic quenching typically intensifies at elevated temperatures due to enhanced molecular collisions. Static quenching often diminishes as an increased temperature destabilizes preformed complexes. To elucidate the mode of interaction between the Cu/Mn/Na polymer and BLC, fluorescence titration data were analyzed using the Stern–Volmer equation (eqn (1)), which facilitates quantitative interpretation of quenching behavior and identification of the predominant interaction mechanism.[17]

$$\frac{F_0}{F} = 1 + k_q\tau_0[Q] = 1 + K_{sv}[Q] \quad (1)$$

The Stern–Volmer equation incorporated several key parameters: the fluorescence intensity of catalase in the absence and presence of the Cu/Mn/Na polymer (denoted as F_0 and F, respectively), the Stern–Volmer quenching constant (K_{SV}), the quencher concentration ([Q]), and the fluorescence lifetime of the enzyme without a quencher, assumed to be 10^{-8} s.[18] Stern–Volmer plots were constructed by graphing F_0/F *versus* [Q] at three temperatures, and are presented in Fig. 5A. From the linear regression of these plots, the K_{SV} was derived, and the bimolecular quenching rate constant (k_q) was subsequently calculated using the equation $K_{SV} = k_q\tau_0$. As summarised in Table 1, K_{SV} and k_q exhibited a decreasing trend with increasing temperature. This inverse relationship supported the notion of predominance of a static quenching mechanism in the interaction between the Cu/Mn/Na polymer and BLC, indicating complex formation rather than collisional quenching.

To quantify the interaction between the Cu/Mn/Na polymer and catalase, the number of binding sites (n) and binding

Open Access Article. Published on 29 July 2025. Downloaded on 12/6/2025 10:08:35 PM.
This article is licensed under a Creative Commons Attribution-NonCommercial 3.0 Unported Licence.

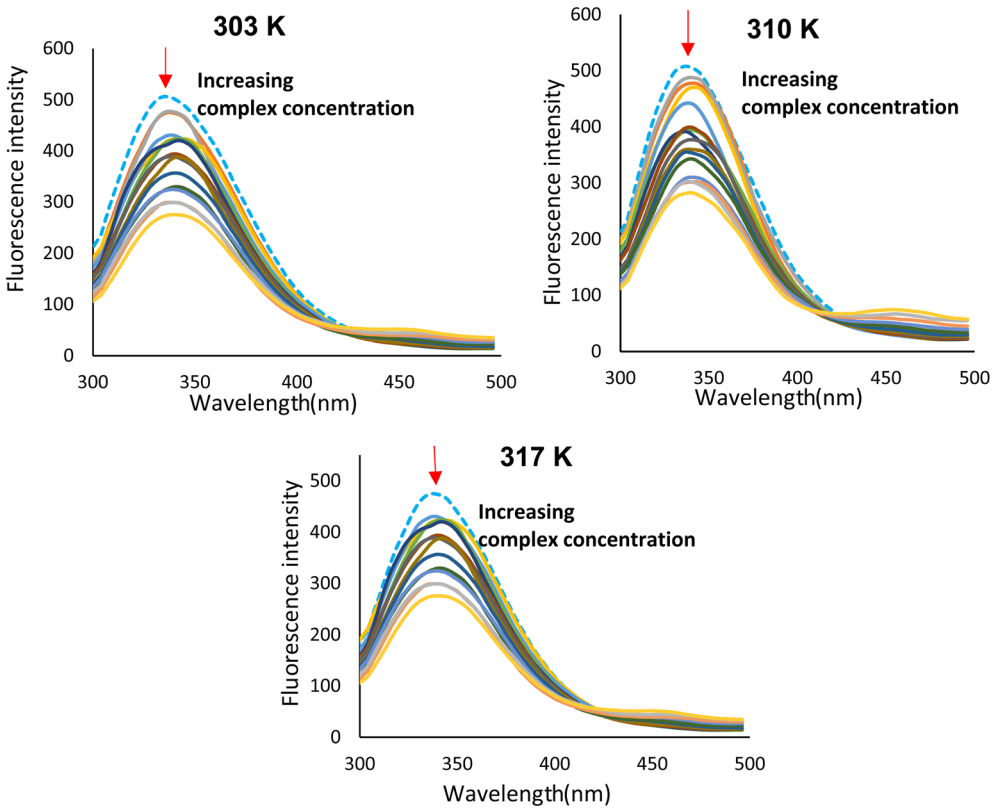

Fig. 4 BLC fluorescence titration before (dashed line) and after (solid lines) interaction with the Cu/Mn/Na polymer at 303, 310 and 317 K. [Polymer] = 0–5.36 × 10^{-5} M.

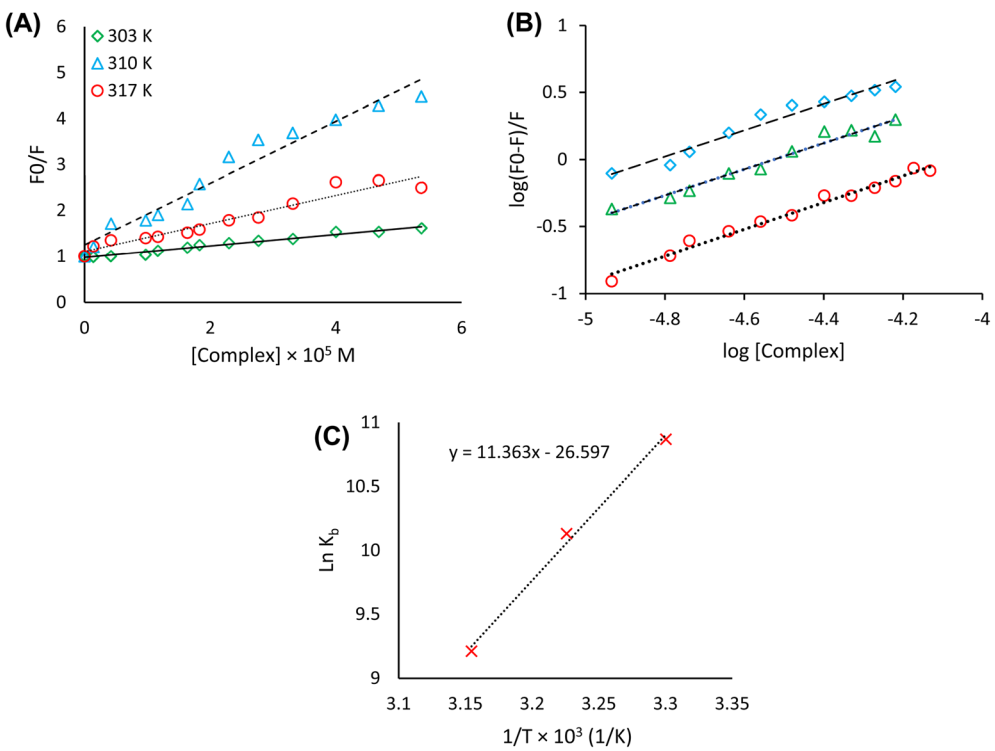

Fig. 5 (A) Stern–Volmer plots of BLC after interaction with the Cu/Mn/Na polymer at 303, 310 and 317 K. (B) Plot of log($F_0 - F/F$) *vs.* log[polymer]. (C) van't Hoff plots.

© 2025 The Author(s). Published by the Royal Society of Chemistry

Open Access Article. Published on 29 July 2025. Downloaded on 12/6/2025 10:08:35 PM. This article is licensed under a Creative Commons Attribution-NonCommercial 3.0 Unported Licence.

Table 1 Interaction parameters in BLC-Cu/Mn/Na polymer

T (K)	n	$K_{sv} \times 10^4$ (M^{-1})	$k_q \times 10^{12}$ (M^{-1} s^{-1})	$K_b \times 10^4$ (M^{-1})	$\Delta G°$ (kJ mol^{-1})	$\Delta H°$ (kJ mol^{-1})	$\Delta S°$ (kJ mol^{-1} K^{-1})
303	1.10	6.71 ± 0.04	6.71 ± 0.04	5.24 ± 0.06	−26.56	−94.77	−0.22
310	0.97	3.08 ± 0.04	3.08 ± 0.04	4.63 ± 0.05	−26.00		
317	0.97	1.21 ± 0.03	1.21 ± 0.03	1.01 ± 0.03	−24.45		

affinity constant (K_b) could be determined using eqn (2), which is commonly applied in studies of ligand–protein binding:[16]

$$\log\frac{F_0 - F}{F} = \log K_b + n\log[Q] \quad (2)$$

Using the plots of $\log\frac{F_0 - F}{F}$ *vs.* log[Q] shown in Fig. 5B, the values of n and the K_b were obtained and are presented in Table 1. The calculated values of n were ~1, suggesting the presence of a single, high-affinity binding site on catalase for the Cu/Mn/Na polymer. A decline in the binding constant (K_b) with increasing temperature suggested involvement of a static quenching mechanism. During the interaction between the Cu/Mn/Na polymer and BLC, the binding constants were found to be in the range of 10^4 M^{-1}. This magnitude suggested a "moderate" binding affinity, comparable with that observed in compounds with established pharmacological activity at the clinical level.[19,20]

Thermodynamic parameters and intermolecular interactions

Binding events between proteins and small molecules are largely stabilised through non-covalent interactions such as hydrogen bonds, van der Waals forces, electrostatic attractions, and hydrophobic effects. These forces, though relatively weak individually, collectively influence binding strength and specificity. The thermodynamic parameters of change in Gibbs free energy (ΔG), enthalpy change (ΔH), and entropy change (ΔS) serve as vital indicators of the nature and spontaneity of molecular interactions, and can be derived from temperature-dependent binding studies.

According to the framework established by Ross and Subramanian[21] the sign and magnitude of ΔH and ΔS can be used to infer the dominant forces stabilising the ligand–protein complex. Specifically, negative values for ΔH and ΔS suggest that hydrogen bonding and van der Waals interactions are primarily responsible for complex formation. Conversely, positive values for both parameters indicate that hydrophobic interactions are the prevailing force. A combination of a negative ΔH and a positive ΔS implies the involvement of electrostatic interactions. The thermodynamic constants, including enthalpy, entropy, and free energy changes, were calculated using van't Hoff and Gibbs–Helmholtz equations, as represented in eqn (3) and (4):

$$\ln K_b = -\frac{\Delta H^\circ}{RT} + \frac{\Delta S^\circ}{R} \quad (3)$$

$$\Delta G^\circ = \Delta H^\circ - T\Delta S^\circ \quad (4)$$

Thermodynamic parameters were derived from the linear fit of the van't Hoff plot, in which the slope and y-intercept of the plot of $\ln K_b$ *versus* $1/T$ (Fig. 5C) correspond to changes in enthalpy (ΔH) and entropy (ΔS), respectively. The calculated values of these parameters are summarised in Table 1. ΔH and ΔS were found to be negative, suggesting that the interaction between catalase and the Cu/Mn/Na polymer was primarily stabilised through hydrogen bonding and van der Waals forces. Furthermore, the values for change in Gibbs free energy (ΔG) were consistently negative across tested temperatures, indicating that the binding was thermodynamically favourable and occurred spontaneously.

Structural alterations in BLC

Synchronous fluorescence spectroscopy serves as an effective method for probing conformational changes in proteins.[22] This method enables the assessment of local environmental polarity around aromatic amino-acid residues, specifically Tyr and Trp, by maintaining fixed wavelength intervals ($\Delta\lambda$) of 15 nm and 60 nm, respectively. Alterations in the maximum emission wavelength (λ_{max}) reflect changes in the polarity of the surrounding microenvironment of these residues. Fig. 6 illustrates the synchronous fluorescence spectra of BLC in the presence of increasing concentrations of the Cu/Mn/Na polymer. A consistent decline in fluorescence intensity was observed with rising polymer levels, indicating the quenching of intrinsic fluorescence. A shift in λ_{max} was not observed for Tyr ($\Delta\lambda = 15$ nm), but the Trp spectrum ($\Delta\lambda = 60$ nm) exhibited a red shift from 279 to 287 nm. This bathochromic shift suggested that the Trp residues were situated in a more polar environment as a result of polymer binding. Consequently, it can be inferred that the Cu/Mn/Na polymer interacted more closely with Trp residues, implying that the binding site was in closer proximity to Trp than to Tyr.[23]

The 3D fluorescence spectra of BLC before and after exposure to the Cu/Mn/Na polymer are displayed in Fig. 7. In its native state, BLC exhibited a broad fluorescence emission centred around 360 nm, along with prominent excitation peaks at approximately 240 nm and 293 nm, labelled as Peaks 1 and 2, respectively. Peak 1 arose from the combined emission of multiple intrinsic fluorophores. Peak 2 was associated with fluorescence originating from the polypeptide backbone. Upon interaction with the Cu/Mn/Na polymer, a notable reduction in the intensity of both peaks was observed, suggesting quenching effects. The diminished intensity of Peak 2, in particular, could

Open Access Article. Published on 29 July 2025. Downloaded on 12/6/2025 10:08:35 PM.
This article is licensed under a Creative Commons Attribution-NonCommercial 3.0 Unported Licence.

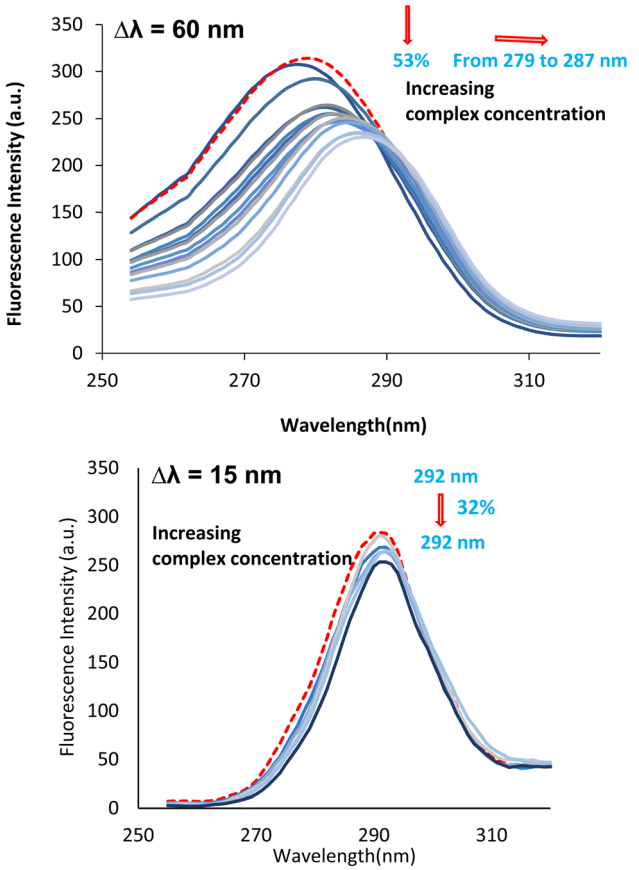

Fig. 6 Synchronous fluorescence spectra of BLC (5×10^{-6} M) before (dash line) and after (solid lines) interaction with the Cu/Mn/Na polymer; [polymer] = 0–5.21×10^{-5} M.

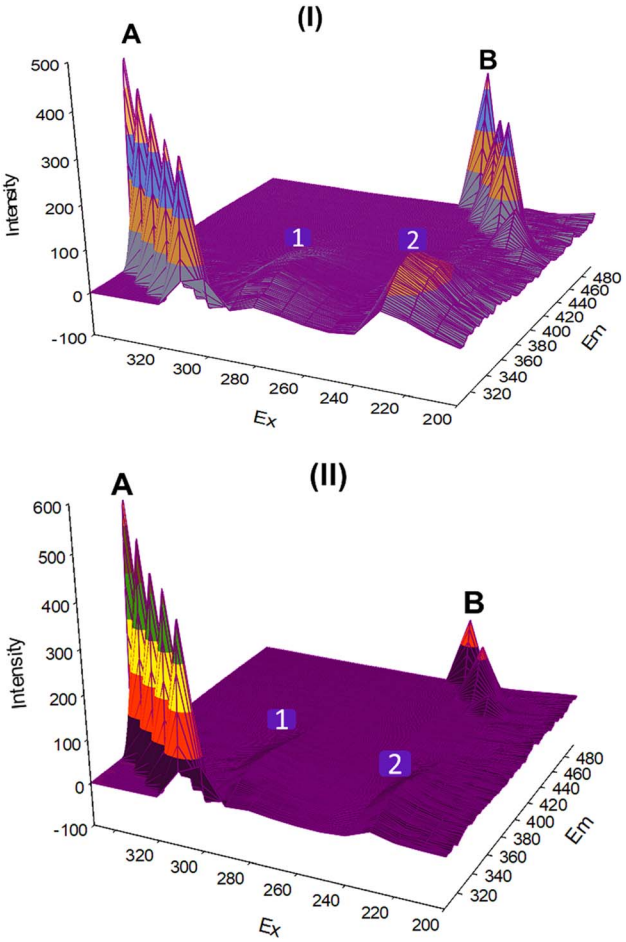

Fig. 7 3D fluorescence spectra of (I) BLC and (II) BLC-Cu/Mn/Na polymer.

be attributed to polymer-induced disruption of the polypeptide chain, resulting in loosening of the overall structure and partial unfolding of the protein backbone.[22] Additionally, Peak 2 demonstrated a slight red shift, indicating an alteration in the polarity of the fluorophore microenvironment, further suggesting structural perturbation. Peak A and Peak B in the spectra represented first- and second-order Rayleigh scattering, respectively.[24]

As shown in Fig. 8, the UV-visible absorption spectrum of the hemoprotein BLC displayed characteristic absorption peaks at 278 nm (corresponding to π–π* transitions in the residues of aromatic amino acids) and ~405 nm (representing the Soret band of the heme moiety). Absorption peaks similar to those of natural BLC occurred at 280 nm for the BLC-Cu/Mn/Na polymer, indicating the possibility of the formation of a BLC-Cu/Mn/Na polymer complex.[25] In addition, the UV absorption intensity increased with an increasing concentration of the Cu/Mn/Na polymer, which may indicate that the hydrophobic groups Trp and Tyr were partially exposed to the interaction between catalase and the Cu/Mn/Na polymer. The maximum absorption peak of catalase shifted to the blue (from 278 to 272 nm), which suggested a change in the polarity around these two amino acids.[26] On the other hand, a negligible change at 405 nm implied that the binding site of the polymer was likely located away from the heme centre, thereby exerting minimal influence on the local environment of the prosthetic group and maintaining the structural integrity of the heme domain.

Antioxidant studies

The antioxidant capacity of the Cu/Mn/Na polymer and vitamin C (Vit C) were studied by the DPPH method (Fig. 9 and S2†).

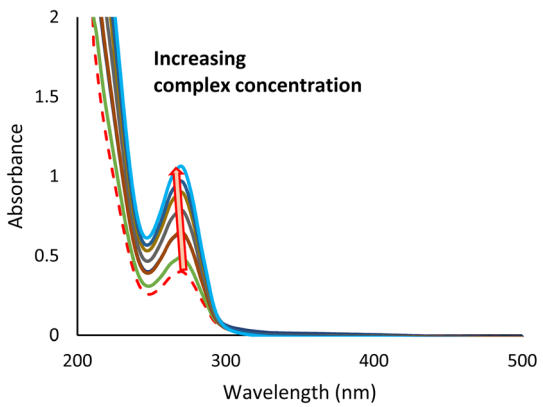

Fig. 8 UV-vis spectra of free BLC (dashed line) (5×10^{-6} M) and BLC-Cu/Mn/Na polymer (solid lines). [Polymer] = 0–5.36×10^{-5} M.

© 2025 The Author(s). Published by the Royal Society of Chemistry

Open Access Article. Published on 29 July 2025. Downloaded on 12/6/2025 10:08:35 PM.
This article is licensed under a Creative Commons Attribution-NonCommercial 3.0 Unported Licence.

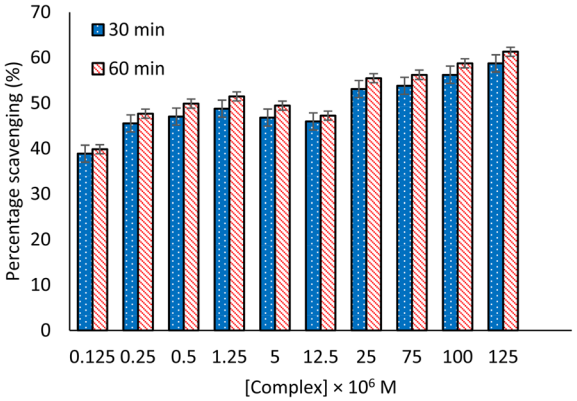

Fig. 9 Antioxidant activity of the Cu/Mn/Na polymer by DPPH• after 30 and 60 min.

Radical scavenging by the Cu/Mn/Na polymer and Vit C at a concentration of 125 μM after 60[30] min was 61.2 (58.7)% and 72.7 (69.3)%,[27] respectively. Although the capacity for scavenging the DPPH free radical of the Cu/Mn/Na polymer was lower than that of standard antioxidants such as Vit C, it showed significant antioxidant properties compared with those of several similar compounds.[28,29] Here, the central metal ion had a critical role in modulating the antioxidant behaviour of the compound. Additionally, the presence of functional groups such as hydroxyl moieties and aromatic ring structures significantly contributes to the overall activity of free radical-scavenging.[19,27,30]

Molecular dynamics simulation

Molecular dynamics simulations enhance the orientation of side chains, leading to an improved structural stability of the model. Through iterative conformational adjustments, the protein structure reaches a more energetically favorable and stable state compared with its initial form. Throughout the simulation, the Cartesian coordinates of each atom are systematically recorded at defined time intervals, creating a trajectory that captures the motion of the system. These structural adjustments result in conformational changes within the macromolecule. By analyzing parameters such as root mean square deviation (RMSD) and root mean square fluctuation (RMSF) relative to the starting structure, one can gain insights into the dynamic behavior, overall stability, and potential interaction mechanisms of a biomolecule.[31,32] Fig. 10A presents the RMSD values of the extracted protein backbones following 100 ns of kinetic simulation. Specifically, RMSD analyses revealed an initial rise in backbone deviation during the first 40 ns, which likely reflected early structural adaptation of the protein to the simulated environment. The subsequent

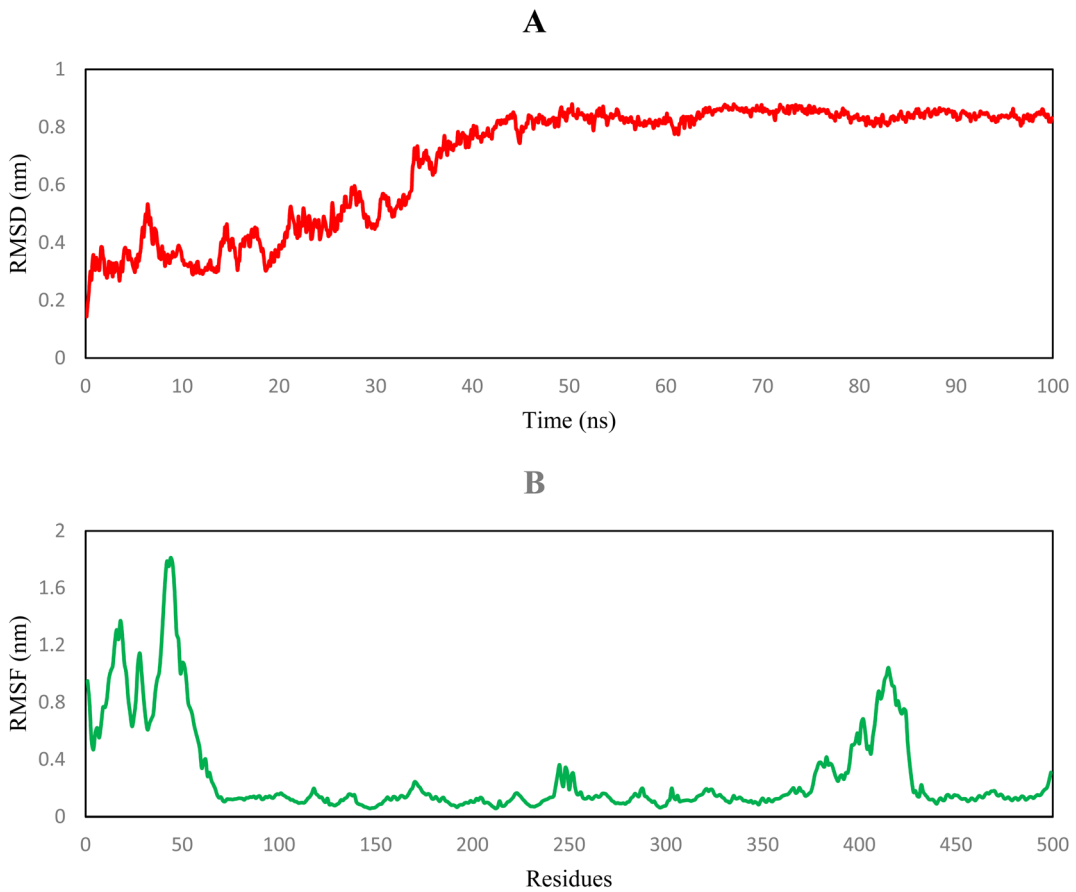

Fig. 10 (A) RMSD (nm) and (B) RMSF (nm) of the backbone atoms of catalase over a 100-ns molecular dynamics simulation.

Open Access Article. Published on 29 July 2025. Downloaded on 12/6/2025 10:08:35 PM.
This article is licensed under a Creative Commons Attribution-NonCommercial 3.0 Unported Licence.

Table 2 Summary statistics of the stereochemical quality of chains A, B, C, and D in the resolved X-ray crystal structure of the BLC complex (PDB code: 1TGU)

Chain A				
All-atom contacts	Clashscore, all atoms	18.96		35th percentile* (N = 1784, all resolutions)
	Clashscore is the number of serious steric overlaps (>0.4 Å) per 1000 atoms			
Protein geometry	Poor rotamers	39	9.05%	Goal: <0.3%
	Favored rotamers	355	82.37%	Goal: >98%
	Ramachandran outliers	3	0.60%	Goal: <0.05%
	Ramachandran favored	452	90.95%	Goal: >98%
	Rama distribution Z-score	−3.82 ± 0.32		Goal: abs(Z score) < 2
	MolProbity score^	3.02		22nd percentile* (N = 27 675, 0–99 Å)
	Cβ deviations >0.25 Å	13	2.80%	Goal: 0
	Bad bonds	6/4137	0.15%	Goal: 0%
	Bad angles	58/5619	1.03%	Goal: <0.1%
Peptide omegas	Cis prolines	1/37	2.70%	Expected: ≤1 per chain, or ≤5%
Low-resolution criteria	CaBLAM outliers	11	2.2%	Goal: <1.0%
	CA geometry outliers	4	0.81%	Goal: <0.5%
Additional validations	Tetrahedral geometry outliers	7		
	Waters with clashes	0/0	0.00%	See UnDowser table for details
Chain B				
All-atom contacts	Clashscore, all atoms	32.96		13th percentile* (N = 1784, all resolutions)
	Clashscore is the number of serious steric overlaps (>0.4 Å) per 1000 atoms			
Protein geometry	Poor rotamers	49	11.37%	Goal: <0.3%
	Favored rotamers	327	75.87%	Goal: >98%
	Ramachandran outliers	8	1.61%	Goal: <0.05%
	Ramachandran favored	419	84.31%	Goal: >98%
	Rama distribution Z-score	−4.64 ± 0.31		Goal: abs(Z score) < 2
	MolProbity score^	3.47		9th percentile* (N = 27 675, 0–99 Å)
	Cβ deviations >0.25 Å	7	1.51%	Goal: 0
	Bad bonds	4/4137	0.10%	Goal: 0%
	Bad angles	32/5619	0.57%	Goal: <0.1%
Peptide omegas	Cis prolines	1/37	2.70%	Expected: ≤1 per chain, or ≤5%
Low-resolution criteria	CaBLAM outliers	20	4.0%	Goal: <1.0%
	CA geometry outliers	7	1.41%	Goal: <0.5%
Additional validations	Tetrahedral geometry outliers	3		
	Waters with clashes	0/0	0.00%	See UnDowser table for details
Chain C				
All-atom contacts	Clashscore, all atoms	24.7		22nd percentile* (N = 1784, all resolutions)
	Clashscore is the number of serious steric overlaps (>0.4 Å) per 1000 atoms			
Protein geometry	Poor rotamers	46	10.67%	Goal: <0.3%
	Favored rotamers	330	76.57%	Goal: >98%
	Ramachandran outliers	8	1.61%	Goal: <0.05%
	Ramachandran favored	434	87.32%	Goal: >98%
	Rama distribution Z-score	−4.30 ± 0.30		Goal: abs(Z score) < 2
	MolProbity score^	3.28		14th percentile* (N = 27 675, 0–99 Å)
	Cβ deviations >0.25 Å	8	1.72%	Goal: 0
	Bad bonds	10/4137	0.24%	Goal: 0%
	Bad angles	37/5619	0.66%	Goal: <0.1%
Peptide omegas	Cis prolines	1/37	2.70%	Expected: ≤1 per chain, or ≤5%
	Twisted peptides	1/498	0.20%	Goal: 0
Low-resolution criteria	CaBLAM outliers	18	3.6%	Goal: <1.0%
	CA geometry outliers	4	0.81%	Goal: <0.5%
Additional validations	Tetrahedral geometry outliers	7		
	Waters with clashes	0/0	0.00%	See UnDowser table for details

© 2025 The Author(s). Published by the Royal Society of Chemistry

Open Access Article. Published on 29 July 2025. Downloaded on 12/6/2025 10:08:35 PM. This article is licensed under a Creative Commons Attribution-NonCommercial 3.0 Unported Licence.

Table 2 (*Contd.*)

Chain D				
All-atom contacts	Clashscore, all atoms	26.47		19th percentile* ($N = 1784$, all resolutions)
	Clashscore is the number of serious steric overlaps (>0.4 Å) per 1000 atoms			
Protein geometry	Poor rotamers	39	9.05%	Goal: <0.3%
	Favored rotamers	345	80.05%	Goal: >98%
	Ramachandran outliers	7	1.41%	Goal: <0.05%
	Ramachandran favored	435	87.53%	Goal: >98%
	Rama distribution *Z*-score	-4.83 ± 0.29		Goal: abs(Z score) < 2
	MolProbity score^	3.15		18th percentile* ($N = 27\,675$, 0–99 Å)
	Cβ deviations >0.25 Å	1	0.22%	Goal: 0
	Bad bonds	2/4137	0.05%	Goal: 0%
	Bad angles	7/5619	0.12%	Goal: <0.1%
Peptide omegas	Cis prolines	1/37	2.70%	Expected: ≤1 per chain, or ≤5%
Low-resolution criteria	CaBLAM outliers	17	3.4%	Goal: <1.0%
	CA geometry outliers	4	0.81%	Goal: <0.5%
Additional validations	Tetrahedral geometry outliers	1		
	Waters with clashes	0/0	0.00%	See UnDowser table for details

stabilization of RMSD values from 40 to 100 ns indicated that the protein reached equilibrium, suggesting that its overall conformation remained stable and suitable for downstream analyses, including docking. RMSF analyses provides insight into residue-level flexibility. As illustrated in Fig. 10B, most residues had RMSF < 0.3 nm, indicating that the core structure of the protein remained rigid and stable during the simulation. This structural rigidity is essential for maintaining catalytic activity and reliable recognition of a ligand. Regions with low fluctuation, particularly residues 190–240 and 270–310, were involved in key interactions such as hydrogen bonding (ARG200, LYS234, ASN241, and TYR277) and hydrophobic contacts (PHE195) with ligands, which reinforced their functional importance and structural stability. In contrast, higher fluctuations observed in the 400–450 region likely corresponded to terminal or loop regions that were naturally more flexible. Such flexibility did not compromise the functional core of the protein, but may have contributed to dynamic conformational changes or interactions with other biomolecules. These observations suggested that the protein maintained structural integrity and functional viability throughout the simulation.

Molecular docking analysis

Molecular docking is a well-established approach for determining the binding interactions between proteins and ligands.[33] The 3D atomic arrangement within a protein molecule (known as its stereochemistry) plays a crucial part in its functionality and interactions with other molecules. To ensure optimal results, various metrics available on the MolProbity web server were employed to evaluate the stereochemical quality of the A, B, C, and D chains in the resolved X-ray crystal structure of the BLC complex (PDB code: 1TGU), as presented in Table 2. Chain A was selected based on several quality metrics. Its clash score was lower than those of chains B, C, and D, indicating fewer steric clashes between atoms. Chains A and D showed comparable percentages of poor rotamers; both lower than those in chains B and C; chain A had the highest percentage of favored rotamers among all four, suggesting more optimal side-chain conformations. Additionally, chain A exhibited a lower Ramachandran outlier score, as well as higher Ramachandran distribution *Z*-score and MolProbity score, compared with those of the other chains. These structural advantages suggested selection of chain A for the docking protocol and subsequent molecular-dynamics simulation.

We used SMINA software to perform the docking of the Cu/Mn/Na polymer with BLC. By default, SMINA utilises the AutoDock Vina scoring function. AutoDock Vina is a widely used docking software that employs an empirical scoring function incorporating steric, electrostatic, solvation, and hydrophobic interactions to evaluate ligand-receptor binding affinities. It employs a gradient-based search algorithm to identify the lowest-energy binding pose within the active site of the receptor. In contrast, SMINA is a modified version (fork) of AutoDock Vina designed to enhance support for development of scoring functions and energy minimization. While it retains the default scoring function of Vina, SMINA allows users to modify and expand the scoring parameters, including additional energetic terms such as electrostatics, desolvation effects, and Lennard-Jones interactions. Molecular-docking simulations revealed that hydrogen bonding and van der Waals forces had crucial roles in facilitating the binding and complex formation between the BLC protein and Cu/Mn/Na polymer. These intermolecular interactions were identified as the primary driving forces responsible for the stable association and binding affinity observed in the BLC-Cu/Mn/Na polymer system by fluorescence studies. During the molecular docking involving the Cu/Mn/Na polymer and BLC protein, SMINA produced nine distinct binding conformations of the polymer with the protein. These conformations were systematically analysed and ranked

Open Access Article. Published on 29 July 2025. Downloaded on 12/6/2025 10:08:35 PM.
This article is licensed under a Creative Commons Attribution-NonCommercial 3.0 Unported Licence.

Table 3 SMINA score of BLC with different conformers of the Cu/Mn/Na polymer

Pose	Affinity of BLC (kJ mol^{-1})
1	−29.7
2	−27.7
3	−27.5
4	−24.4
5	−22.9
6	−21.9
7	−21.3
8	−20.7
9	−20.5

according to their calculated affinity scores, as detailed in Table 3. Among the various conformations explored, the highest binding affinity observed for the polymer interacting with the BLC protein was −29.7 kJ mol^{-1}, indicating a favorable and stable binding interaction. The structure of catalase could be divided into four domains: an N-terminal arm (residues 1–70), which formed two α-helices and a large loop extending from the globular core; a heme-binding domain (residues 71–318), centered around an anti-parallel eight-stranded β-barrel flanked by helices and loops; a wrapping domain (residues 319–439), containing two helices within largely unstructured regions; a C-terminal domain (residues 440–501), which folded into a four-helix bundle. This structural arrangement is shown in Fig. 11A. As illustrated, the interaction of the best binding pose of the polymer with BLC, as well as its position relative to the heme group, was investigated using molecular docking. The calculated binding energy values for the nine conformational poses explored ranged from −29.7 to −20.5 kJ mol^{-1}. These computational estimates are in close agreement with the previously reported experimental value of −26.56 kJ mol^{-1} for ΔG° associated with this binding interaction. The binding interactions between the Cu/Mn/Na polymer and specific amino-acid residues of the BLC protein were investigated using Discovery Studio Visualizer 2021 (Fig. 11). Computational analyses revealed that the polymer formed hydrogen bonds with the side chains of ARG200, LYS234, ASN241, and TYR277 residues. Additionally, van der Waals interactions were observed between the polymer and amino-acid residues ASP210, TYR212, and LEU307. Furthermore, PHE195 formed a hydrophobic interaction with the polymer. The bond lengths for hydrogen bonds and hydrophobic interaction are shown in Fig. 11.

Cytotoxic assessment using MTT assay

As a supplementary study, the impact of the Cu/Mn/Na polymer on colon cancer (HCT116) cells was investigated as a preliminary step towards future research. Cisplatin, a commonly used cancer treatment, was used for comparison. Fig. 12A revealed that Cu/Mn/Na polymer concentrations >250 μM could inhibit the growth of HCT116 cancer cells, with its efficacy matching that of cisplatin within this concentration range. However, at lower concentrations, cisplatin demonstrated superior performance. Therefore, it can be inferred that Cu/Mn/Na polymer inhibited cancer-cell growth in a concentration- and time-dependent manner, whereas the cytotoxic effects of cisplatin were solely time-dependent. The IC_{50} values for the Cu/Mn/Na polymer at 48 and 72 h were estimated to be 208 and 123 μM, respectively whereas, for cisplatin, they were 41 and 33 μM.

To investigate the effect of the polymer on normal cells, NIH/3T3 fibroblasts were exposed to six concentrations of the Cu/

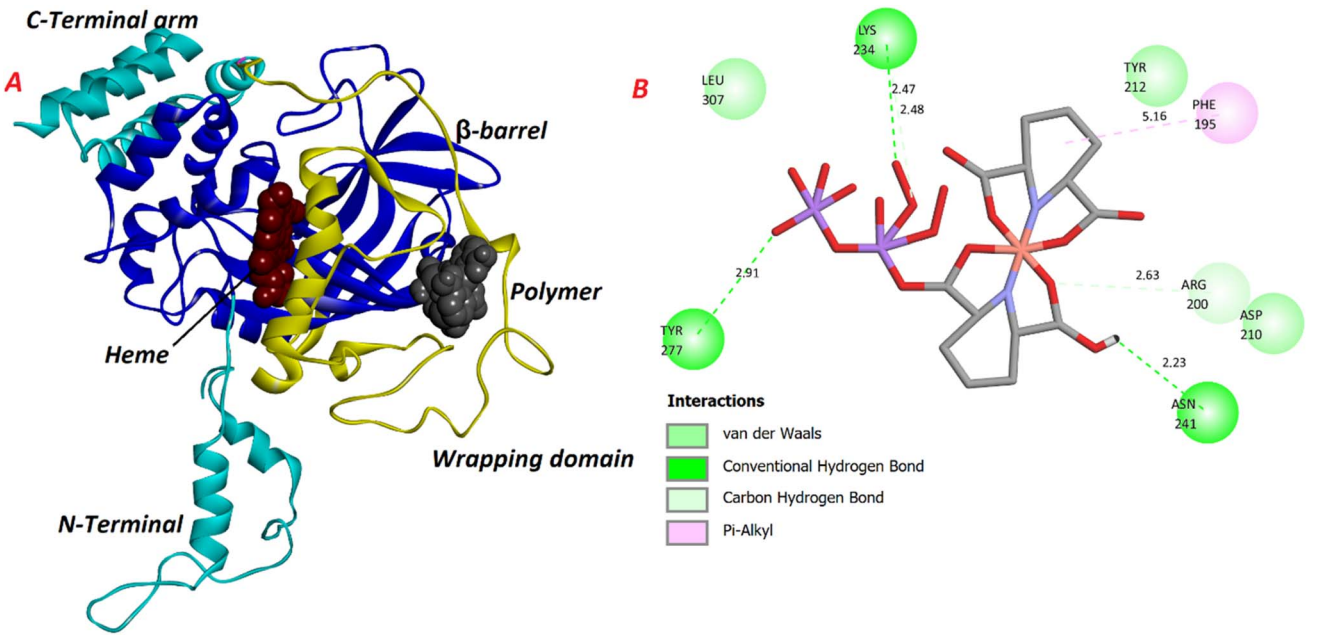

Fig. 11 (A) 3D and (B) 2D representations of the molecular-docking results obtained using SMINA. Images were created with Discovery Studio Visualizer.

© 2025 The Author(s). Published by the Royal Society of Chemistry

Open Access Article. Published on 29 July 2025. Downloaded on 12/6/2025 10:08:35 PM.
This article is licensed under a Creative Commons Attribution-NonCommercial 3.0 Unported Licence.

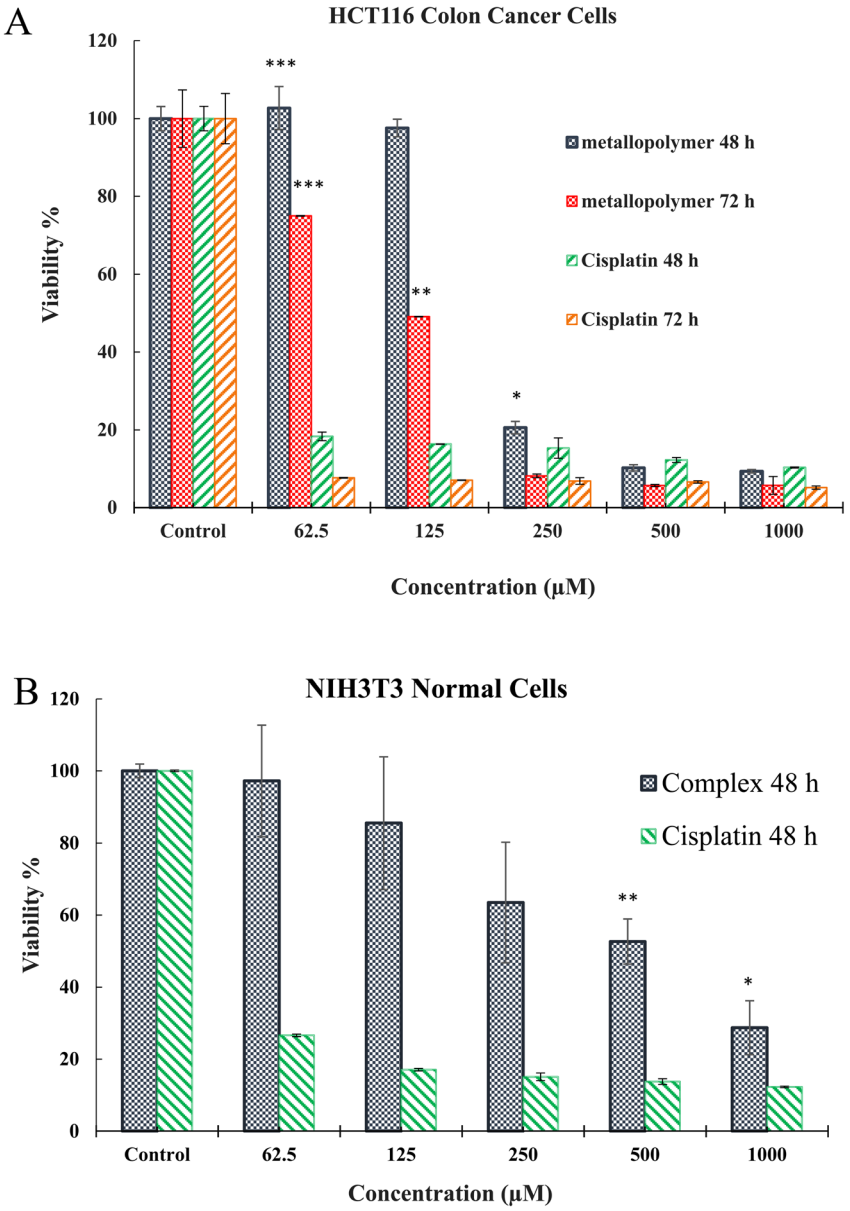

Fig. 12 (A) The toxic effects of the Cu/Mn/Na polymer and cisplatin were evaluated on colon cancer (HCT116) cells following 48 or 72 h of treatment. (B) The toxic impact of the Cu/Mn/Na polymer and cisplatin on NIH/3T3 fibroblasts was assessed after 48 h of exposure. Data were analyzed using one-way analysis of variance (ANOVA) followed by Tukey's *post hoc* test, with statistical significance defined as $P < 0.05$.

Mn/Na polymer for 48 h, and results compared with data for cisplatin. As shown in Fig. 12B, the polymer was able to reduce cell viability to <50% at a concentration of 1000 μM, whereas cisplatin was toxic to normal cells at all concentrations. For deeper understanding, the IC_{50} values of the Cu/Mn/Na polymer after 48 h (570 μM) and cisplatin (43 μM) were measured, and indicated the significant effect of cisplatin on the death of normal cells compared with that of the polymer.

A major reason for these results is the larger size of the synthesized polymer compared with cisplatin. The polymer can pass through the large pores of cancer cells that are formed due to defective angiogenesis,[34] whereas it is unable to pass through the pores of normal cells and can cause the death of only normal cells at increasing concentrations. Therefore, the polymer could kill colon cancer cells at an optimal concentration of ~200 μM while remaining safe for normal cells.

Conclusions

We revealed the molecular mechanism behind the enhanced activity of BLC upon exposure to the Cu/Mn/Na polymer. Results were presented through a variety of biophysical methods. Assessment of antioxidant activity *via* the ˙DPPH assay revealed that the Cu/Mn/Na polymer could inhibit free radicals. The interaction of the Cu/Mn/Na polymer with BLC showed that it could improve enzyme activity. An enhancement in enzymatic activity can often be attributed to structural modifications that result in increased accessibility of the substrate-binding

Open Access Article. Published on 29 July 2025. Downloaded on 12/6/2025 10:08:35 PM. This article is licensed under a Creative Commons Attribution-NonCommercial 3.0 Unported Licence.

channel within an active site. It is likely that stronger interactions between the enzyme and interacting compound promote more pronounced conformational changes, thereby facilitating substrate entry and subsequently increasing catalytic efficiency. This ability can lead to improvement of the antioxidant immune system of the body. The interaction between the Cu/Mn/Na polymer and BLC was predominantly stabilised by van der Waals forces and hydrogen bonding. Overall, the development and study of metal-based complexes are promising for chemotherapy and they could become therapeutic agents. The Cu/Mn/Na polymer could inhibit the growth of colon cancer (HCT116) cells in a concentration- and time-dependent manner, whereas its toxic impact upon normal cells was significantly lower than that of cisplatin.

Abbreviations

DPPH	2,2-Diphenyl-1-picrylhydrazyl
ROS	Reactive oxygen species
BLC	Bovine liver catalase
K_{SV}	Stern–Volmer quenching constant
n	Number of ligand binding sites on catalase
K_b	Binding constant

Data availability

The crystal structure of BLC was obtained from the Protein Data Bank (**https://www.rcsb.org/pdb/home/home.do/**, code: 1TGU), whereas the structure of the Cu/Mn/Na polymer was retrieved from the Cambridge Crystallographic Data Centre (**https://www.ccdc.cam.ac.uk/**, CCDC-2072192). The other data that support the findings of this study are available within the article.

Author contributions

Narges Lashkarzade: performed experiments and investigations. Fereshteh Shiri: initiated the research, led the project team, conducted the computational study, and contributed to writing, reviewing, and editing the manuscript. Somaye Shahraki: assisted in resolving experimental technical issues, conducted data analyses, and contributed to manuscript writing. Zohreh Razmara: synthesized the Cu/Mn/Na polymer and contributed to writing the manuscript. Mostafa Heidari Majd: conducted the MTT assay and contributed to writing the manuscript.

Conflicts of interest

The authors declare that there is no conflict of interest regarding publication of this article.

Acknowledgements

This work was funded by the University of Zabol (IR-UOZ-GR-0144).

References

1 F. Jäkle, Advances in the synthesis of organoborane polymers for optical, electronic, and sensory applications, *Chem. Rev.*, 2010, **110**(7), 3985–4022.
2 R. Resendes, J. M. Nelson, A. Fischer, F. Jäkle, A. Bartole, A. J. Lough, *et al.*, Tuning the Strain and Polymerizability of Organometallic Rings: The Synthesis, Structure, and Ring-Opening Polymerization Behavior of [2] Ferrocenophanes with C–Si, C–P, and C–S Bridges, *J. Am. Chem. Soc.*, 2001, **123**(10), 2116–2126.
3 Y. Yan, J. Zhang, L. Ren and C. Tang, Metal-containing and related polymers for biomedical applications, *Chem. Soc. Rev.*, 2016, **45**(19), 5232–5263.
4 M. Wang, X. Wang, J. Sun, Z. Nie, W. He, H. Sai, *et al.*, The interaction between resveratrol and catalase was studied by multispectral method and molecular docking simulation, *J. Mol. Struct.*, 2025, **1321**, 139720.
5 C. Glorieux and P. B. Calderon, Targeting catalase in cancer, *Redox Biol.*, 2024, 103404.
6 Z. Razmara, V. Eigner and M. Dusek, Single crystal structure features of a new tri-hetero metallic polymer, a catalyst for mild homogeneous peroxidative oxidation of cyclohexane, *J. Solid State Chem.*, 2022, **311**, 123123.
7 S. Khataee, G. Dehghan, R. Yekta, S. Rashtbari, S. Maleki and A. Khataee, The protective effect of natural phenolic compound on the functional and structural responses of inhibited catalase by a common azo food dye, *Food Chem. Toxicol.*, 2022, **160**, 112801.
8 Z. Cao, R. Liu and B. Yang, Potential toxicity of sarafloxacin to catalase: spectroscopic, ITC and molecular docking descriptions, *Spectrochim. Acta, Part A*, 2013, **115**, 457–463.
9 R. Yekta, G. Dehghan, S. Rashtbari, R. Ghadari and A. A. Moosavi-Movahedi, The inhibitory effect of farnesiferol C against catalase; Kinetics, interaction mechanism and molecular docking simulation, *Int. J. Biol. Macromol.*, 2018, **113**, 1258–1265.
10 J. Zhang, L. Chen, Y. Zhu and Y. Zhang, Study on the molecular interactions of hydroxylated polycyclic aromatic hydrocarbons with catalase using multi-spectral methods combined with molecular docking, *Food Chem.*, 2020, **309**, 125743.
11 S. Shahraki, Z. Razmara and F. Shiri, A paramagnetic oxalato-bridged binuclear copper (II) complex as an effective catalase inhibitor. Spectroscopic and molecular docking studies, *J. Mol. Struct.*, 2020, **1208**, 127865.
12 B. Baral, P. S. Nial and U. Subudhi, Enhanced enzymatic activity and conformational stability of catalase in presence of tetrahedral DNA nanostructures: A biophysical and kinetic study, *Int. J. Biol. Macromol.*, 2023, **242**, 124677.
13 D.-F. Zhou, Q.-Y. Chen, Y. Qi, H.-J. Fu, Z. Li, K.-D. Zhao, *et al.*, Anticancer activity, attenuation on the absorption of calcium in mitochondria, and catalase activity for manganese complexes of N-substituted di (picolyl) amine, *Inorg. Chem.*, 2011, **50**(15), 6929–6937.

© 2025 The Author(s). Published by the Royal Society of Chemistry

Open Access Article. Published on 29 July 2025. Downloaded on 12/6/2025 10:08:35 PM. This article is licensed under a Creative Commons Attribution-NonCommercial 3.0 Unported Licence.

14 T. P. Silverstein, When both Km and Vmax are altered, Is the enzyme inhibited or activated?, *Biochem. Mol. Biol. Educ.*, 2019, **47**(4), 446–449.
15 A. Saboury, Enzyme inhibition and activation: a general theory, *J. Iran. Chem. Soc.*, 2009, **6**, 219–229.
16 S. Rashtbari, G. Dehghan, L. Sadeghi, L. Sareminia, M. Iranshahy, M. Iranshahi, *et al.*, Interaction of bovine serum albumin with ellagic acid and urolithins A and B: Insights from surface plasmon resonance, fluorescence, and molecular docking techniques, *Food Chem. Toxicol.*, 2022, **162**, 112913.
17 M. R. Eftink and C. A. Ghiron, Fluorescence quenching studies with proteins, *Anal. Biochem.*, 1981, **114**(2), 199–227.
18 U. Noomnarm and R. M. Clegg, Fluorescence lifetimes: fundamentals and interpretations, *Photosynth. Res.*, 2009, **101**, 181–194.
19 O. Barani, S. Shahraki, Z. S. Nezami, H. S. Delarami and E. Sanchooli, Unveiling the molecular association of novel benzohydrazide-substituted Schiff base complexes with human serum albumin, *Inorg. Chem. Commun.*, 2024, **162**, 112200.
20 M. Hashemizadeh, F. Shiri, S. Shahraki and Z. Razmara, A multidisciplinary study for investigating the interaction of an iron complex with bovine liver catalase, *Appl. Organomet. Chem.*, 2022, **36**(11), e6881.
21 P. D. Ross and S. Subramanian, Thermodynamics of protein association reactions: forces contributing to stability, *Biochemistry*, 1981, **20**(11), 3096–3102.
22 X. Li, L. Han, Z. Song, R. Xu and L. Wang, Comparative study on the interaction between transferrin and flavonols: experimental and computational modeling approaches, *Spectrochim. Acta, Part A*, 2023, **288**, 122128.
23 X. f. Zhang, L. Lan, L. Chen, H. b. Chen, Q. f. Yang, Q. Li, *et al.*, Spectroscopic investigation on the binding of a cyanine dye with transferrin, *J. Phys. Org. Chem.*, 2016, **29**(3), 127–133.
24 W. Li, X. Li, C. Han, L. Gao, H. Wu and M. Li, A new view into three-dimensional excitation-emission matrix fluorescence spectroscopy for dissolved organic matter, *Sci. Total Environ.*, 2023, **855**, 158963.
25 S. Shahraki, H. S. Delarami, H. Mansouri-Torshizi and H. Nouri, Investigation of kinetics and thermodynamics in the interaction process between two pyridine derived Schiff base complexes and catalase, *J. Mol. Liq.*, 2021, **334**, 116527.
26 A. O. Keikha, H. Mansouri-Torshizi, S. Shahraki and E. Dehghanian, Zn (II) and Pd (II) complexes derived from novel benzohydrazide-based Schiff base ligand as multi-target agents, *J. Mol. Liq.*, 2023, **391**, 123272.
27 K. Shahraki, S. Shahraki, Z. S. Nezami and H. S. Delarami, New acetohydrazide-based Schiff base complexes with the ability to enhance catalase activity, *Inorg. Chem. Commun.*, 2024, **163**, 112318.
28 H. Nouri, H. Mansouri-Torshizi and S. Shahraki, Exploring the functional changes and binding mechanism of bovine liver catalase in the presence of Schiff base complexes. Comprehensive spectroscopic studies, *J. Iran. Chem. Soc.*, 2021, **18**(12), 3281–3294.
29 S. Shahraki, F. Shiri and Z. Razmara, Improving enzymatic performance of antioxidant enzyme catalase in combination with [Mn (phen) 2Cl. H2O] Cl. tu complex, *Appl. Organomet. Chem.*, 2023, **37**(4), e7061.
30 S. Shahraki, E. Dehghanian and K. Shahraki, Evaluation of anticancer capacity, catalase interactions, molecular docking, and antioxidant studies of some diamagnetic (Pd, Pt, and Zn) Schiff base complexes, *Inorg. Chim. Acta*, 2025, **581**, 122642.
31 Q. Chen, Y. Xiao, E. I. Shakhnovich, W. Zhang and W. Mu, Semi-rational design and molecular dynamics simulations study of the thermostability enhancement of cellobiose 2-epimerases, *Int. J. Biol. Macromol.*, 2020, **154**, 1356–1365.
32 V. Gramany, F. I. Khan, A. Govender, K. Bisetty, S. Singh and K. Permaul, Cloning, expression, and molecular dynamics simulations of a xylosidase obtained from Thermomyces lanuginosus, *J. Biomol. Struct. Dyn.*, 2016, **34**(8), 1681–1692.
33 A. Abdolmaleki, F. Shiri and J. B. Ghasemi, Use of molecular docking as a decision-making tool in drug discovery, *Molecular Docking for Computer-Aided Drug Design*, Elsevier, 2021, pp. 229–243.
34 M. Heidari Majd, K. Behrouz Moghadam and H. Wang, Increasing apoptosis induction and minimizing side effects of biosynthesized silver nanoparticles by utilizing halloysite nanotubes containing folic acid, *Cancer Nanotechnol.*, 2025, **16**(1), 6.